Numerical Methodology Based on Fluid-Structure Interaction to Predict the Residual Stress Distribution in Glass Tempering Considering Non-Uniform Cooling

A. Iglesias[a,b,*], M. Martinez-Agirre[b], I. Torca[a], I. Llavori[a], J. A. Esnaola[a]

[a] *Structural Mechanics and Design, Engineering Faculty, Mondragon Unibertsitatea, Arrasate-Mondragon, Spain*
[b] *Fluid Mechanics, Engineering Faculty, Mondragon Unibertsitatea, Arrasate-Mondragon, Spain*

Abstract

In this paper a novel numerical methodology for calculating non-uniform residual stress distributions during the glass tempering process is presented. Tempering techniques lead to non-uniform heat transfer rates causing residual stress inhomogeneities, which consequently have a direct impact on the structural behaviour of components. Nevertheless, most of the works in the literature do not consider the influence of local flow phenomena during thermal calculations, resulting in non-representative residual stress distributions. In this context, a novel generalized methodology based on a fluid-structure interaction one-way approach to sequentially couple the thermal and mechanical fields is presented. This way, the unsteady and non-uniform heat transfer rate is coupled with the Narayanaswamy model to predict the non-homogeneous residual stress pattern. The obtained numerical results for the analysed impinging jet array case are in good agreement both quantitatively and qualitatively, exhibiting an average error below 10% with respect to previous experimental investigations. Finally, efforts are made to reduce the computational time and therefore, the proposed methodology proves to be an efficient tool for understanding the underlying mechanisms and predicting the residual stress distributions during glass tempering.

Keywords: Fluid-structure interaction, glass tempering, residual stresses, inhomogeneities, volumetric radiation

Nomenclature

Greek letters

a_λ	Spectral absorption coefficient
α_g	Solid glass expansion coefficient
α_l	Liquid glass expansion coefficient
δ	Kronecker delta
ϵ	Turbulence dissipation

*Corresponding author at: Mondragon Unibertsitatea, Loramendi 4, Arrasate-Mondragon, 20500, Spain
Email address: aiglesias@mondragon.edu (A. Iglesias), mmartinez@mondragon.edu (M. Martinez-Agirre), itorca@mondragon.edu (I. Torca), illavori@mondragon.edu (I. Llavori), jaesnaola@mondragon.edu (J. A. Esnaola)

ε	Trace of the strain tensor
ϵ_{th}	Thermal strain
λ	Wavelength
μ	Dynamic viscosity of the fluid phase
μ_{g}	Dynamic viscosity of glass
ξ	Scaled time
ρ	Density
ρ_{g}	Density of glass
σ_{sc}	Scattering coefficient
σ	Absolute maximum principal stress
$\boldsymbol{\sigma}$	Stress tensor
$\boldsymbol{\tau}_{\mathbf{v}}$	Viscous stress tensor
ϕ	Shift factor
Φ	Phase function
ω	Turbulence specific dissipation rate
Ω	Solid angle

Symbols

$c_{\mathrm{p,g}}$	Specific heat of glass
e	Internal energy
$\boldsymbol{e}$	Deviatoric strain tensor
$\vec{F}$	External body force
$G(t)$	Shear relaxation modulus
G_λ	Absorbed irradiation intensity
$\vec{g}$	Gravitational acceleration
H	Activation energy
H_{g}	Thermal activation energy
H_{s}	Structural activation energy
h	Heat transfer coefficient
I_λ	Spectral radiative intensity
$I_{\mathrm{b},\lambda}$	Spectral blackbody intensity
$K(t)$	Bulk modulus
k	Turbulent kinetic energy
$k_{\mathrm{th,f}}$	Thermal conductivity of the fluid

$k_{\mathrm{th,g}}$	Thermal conductivity of glass
M_{p}	Response function of a given property
n	Refractive index
p	Static pressure
$\dot{q}$	Volumetric heat generation
$\mathrm{R_g}$	Universal gas constant
$\vec{r}$	Position vector
$\vec{s}$	Direction vector
$\vec{s'}$	Scattering direction vector
S_{h}	Sources of energy
T_0	Initial temperature
T_∞	Ambient temperature
T_{B}	Reference temperature
T_{cri}	Critical temperature
T_{f}	Fictive temperature
T_{g}	Glass transition temperature
t	Time
t_0	Initial time
t_∞	Steady state time
t_{cri}	Critical time
$\vec{v}$	Velocity vector
y^+	Wall Y plus

Abbreviations

CFD	Computational Fluid Dynamics
DOM	Discrete Ordinates Method
FEA	Finite Element Analysis
FEM	Finite Element Method
FSI	Fluid-Structure Interaction
GEKO	Generalized k-ω turbulence model
HTC	Heat Transfer Coefficient
RS	Residual stress
RTE	Radiative Transfer Equation
SCALP	Scattered Light Polariscope

SST Shear Stress Transport

1. Introduction

Glass components have become ubiquitous in structural applications, covering a wide range of industries, such as the construction and automotive sectors. Nevertheless, glass is strong under compressive actions but shows a weak resistance when subjected to tensile loads. The reason for holding this view relied on the presence of flaws or defects on the surface, which act as stress concentrators [1]. Therefore, unlike ductile materials, brittle materials are unable to redistribute these stresses, resulting in crack growth and propagation until the fracture of the material [2]. Consequently, with the view to strengthening the material and avoid crack propagation, glass is most often heat treated before being used as a structural material.

Glass is annealed with the intention of minimising or eliminating the tensile residual stresses developed during the manufacturing process. With the aim of achieving the required tensile strength though, the tempering process has to be applied. Here, the control of the residual stress development is crucial and numerical methods have gained significant traction. Two main aspects are distinguished when it comes to residual stress calculation in glass components, namely, the structural or material field and the heat transfer modelling. The material modelling and the origin of residual stresses in glass have been deeply studied in literature. Adams & Williamson described the first analytical equation for uniformly cooled glass sheets [3]. From this point on, additional models for non-uniform cooling processes, such as the tempering process, were proposed [4, 5]. Following the works based on the thermoelastic theory, Lee et al. presented a viscoelastic model to predict not only the residual stress distribution but also the transient stress distributions [6]. However, the model was not able to fit the experimental data when quenching the material at low quenching temperatures. Narayanaswamy & Gardon [7] improved the thermoviscoelastic model but it was not until 1971 when Narayanaswamy proposed an extension of the viscoelastic model adding the structural relaxation phenomenon of glass [8]. Moreover, this effect was shown to be a meaningful contributor to the residual stress development during the glass cooling process [9].

On the other hand, the heat transfer modelling is a key factor in the prediction of residual stresses in glass as they are largely influenced by the thermal history of the components. During the glass tempering process, where large heat transfer rates are obtained, the heat transfer mechanisms involved refer to conduction, convection and radiation. Conduction is usually well understood as it is characterized by the thermal conductivity of the material [10]. Regarding convection phenomena, the definition of constant and uniform heat transfer coefficients (HTCs) has been a commonly adopted approach due to its associated low computational cost. Daudeville & Carre presented a FEM model to calculate the residual stress development in glass plates based on the definition of constant HTCs [11, 12]. Bernard et al. conducted a thermal characterization in aluminium plates by thermocouples to resemble the heat extraction in glass during tempering [13, 14]. In this manner, they determined the local HTC for different

areas of the plate: top surface, edge and hole surface. Nielsen et al. performed a parametric study to observe the influence of geometrical features, such as, plate thickness or hole diameter, on the residual stress development near holes [15]. To this end, the authors defined convective HTCs on the glass surface based on the aforementioned study of Daudeville & Carre [12]. Similarly, Pourmoghaddam et al. carried out more exhaustive parametric studies about the behaviour of residual stresses near geometrical discontinuities [16, 17]. They relied on the HTCs obtained by Bernard & Daudeville to perform the thermal calculations [14]. In a more recent work, Pourmoghaddam et al. presented an inverse analysis to determine the needed engine power in order to reach a specific residual stress magnitude by air quenching [18]. The authors performed axisymmetric simulations to calculate the required HTC for the desired degree of temper. Overall, the main shortcoming in the numerical modelling of heat treatment processes is to neglect the local flow phenomena and to approximate it by uniform and constant HTCs over time. Conversely, Mikkonen et al. proposed a simplified approach by using time-constant but spatially different HTC distributions for analysing the effect of different jet configurations on a moving plate [19]. This assumption might enable a further reduction of the computational cost. However, as the transient nature of the turbulent flow is simplified, its influence on the adopted tempering configuration needs to be assessed.

The assumptions of homogeneous and constant HTCs hinders the consideration of non-uniform cooling distributions, which have a direct impact on the residual stress distributions as emphasized by Monnoyer & Lochegnies [20]. Additionally, Nielsen et al. accomplished residual stress measurements on commercially tempered glass plates with different thicknesses by a portable scattered light polariscope (SCALP) [21]. They concluded that more knowledge about the control of the heat treatment process was needed as they observed high variations not only in the residual stress state of individual specimens, but also among specimens of the same batch. A similar statement was made by Anton et al., who measured the residual stress pattern by SCALP and concluded that highly non-uniform distributions were observed [22]. Likewise, Chen et al. carried out an experimental investigation about the uniformity of residual stresses in tempered glass plates [23]. They concluded that too spaced cooling jets might lead to residual stress inhomogeneity and that oscillation of the glass specimen could improve the cooling flow homogeneity. Last but not least, Mikkonen et al. and Karvinen et al. analysed the importance of heat transfer control on the quality of glass in terms of optical anisotropy [19, 24]. The authors highlighted the use of numerical methods to solve the HTC distributions developed by jet impingement. With the aim of facing this challenge, Aronen numerically analysed the effect of HTC and other several process parameters on the residual stress development by a cost-effective one dimensional model [25, 26]. All these authors not only emphasized the need to control heat transfer during tempering, but also mentioned shortages regarding the numerical modelling, such as, the complexity of modelling the interaction of multiple impingement jets and the large amount of computational resources required. Additionally, the application of novel cooling techniques, which in turns demand more sophisticated numerical approaches, is becoming popular within the heat treatment industry. With the view to enhancing the quality of the products or reducing the manufacturing costs, new processes, such as, pulsed jets, swirling jets or interrupt quenching techniques encompassing the use of mist cooling might be encountered [27, 28, 29]. In this sense, modelling the turbulent flow and its interaction with

the target surface become the major challenge for understanding the involved underlying mechanisms and the developed transient boundary layer. For this reason, a generalized 3D numerical methodology that enables to understand the involved multiphysic phenomena and aids in designing and controlling different cooling configurations becomes relevant.

Furthermore, according to the high temperature of the process, not only the convective heat transfer is important, but thermal radiation in semi-transparent media also gains special relevance. Indeed, it can play a vital role on the temperature calculation as it helps to redistribute the heat through the component [30, 31]. According to Siegel, this fact might have a direct impact on the residual stress development during the manufacturing or heat treatment processes [32]. Recently however, some authors stated that the contribution of radiation decreased as the cooling rate increased [33, 34]. Even though, as works focused on this topic relied on 1D calculations, its importance and effect on the spatial residual stress distribution was not clarified yet.

Overall, numerical methods for predicting residual stresses have gained significant traction. Regarding the structural field, the Narayanaswamy structural model was found to be well established as it has been experimentally validated and employed by several authors. Historically however, the influence of local flow phenomena during thermal calculations has not been considered, resulting in non-representative residual stress distributions. In this context, a sequentially coupled fluid-structure interaction (FSI) approach is proposed to predict the residual stress distribution considering the effect of non-uniformities in the cooling process. In this sense, computational fluid dynamics (CFD) becomes a powerful tool that allows capturing the effect of flow behaviour in the heat exchange along the heat treated surface. Consequently, a non-constant heat transfer rate in space and time enabled the calculation of non-uniform residual stress patterns developed during the tempering process. Therefore, this work presents a generalized numerical methodology to predict the non-uniform residual stress distributions during the glass tempering process. Likewise, the proposed numerical procedure not only is considered to be suitable for understanding and designing the novel cooling configurations that the heat treatment industry is facing, but it also accounts for the main drawback of heat treatment simulation, which refers to the involved large computational cost.

The work is organised as follows. Section 2 presents the FSI one-way based methodology and a review of the fundamentals of the involved physics. Similarly, a modified procedure for reducing the computational cost is presented. In Section 3, the application to the tempering process of a flat glass plate is shown. Here, the experimental and numerical case studies are delineated and a mesh sensitivity analysis is carried out. Once the mesh is checked, different computational cost reduction techniques are evaluated. In Section 4, the validation of the predicted residual stresses is performed. A discussion of the obtained numerical results is done by comparing them to previous experimental investigations available in literature. Finally, the main conclusions are summarised in Section 5.

2. Numerical procedure

One of the main limitations in most of the works focused on the residual stress prediction during heat treatment processes regards to the definition of constant and uniform HTCs over time. As a result, non-representative residual stress distributions might be achieved. Generally, heat treated components do not show uniform residual stress patterns due to the employed cooling technique, mainly composed by air jet arrays. The influence of a non-uniform cooling however, it is generally not considered even if the thermal history of the material is known to play a vital role on the residual stress development, especially, in glass components. Therefore, the proposed FSI one-way procedure intends to capture the effect of non-uniform cooling to predict the residual stress magnitude and distribution on heat treated components. The procedure consists of the following steps:

1. **Thermal history calculation:** firstly, a CFD model, where the conduction, convection and radiation phenomena are considered, needs to be defined. Here, the material physical, thermal and optical properties as well as the turbulence and radiation models are defined. To this end, the commercial CFD program Ansys Fluent is used for carrying out the calculation.

2. **Structural model considering the structural relaxation of glass:** subsequently, the calculated temperature distribution are transferred into the commercial Finite Element Analysis (FEA) software Abaqus FEA. The structural model considers the viscoelasticity and structural relaxation phenomena of glass based on the Narayanaswamy model. Its implementation in a 3D algorithm for finite element calculation can be found in the study of Nielsen [35].

3. **Non-uniform RS prediction:** once the part is cooled down to ambient temperature and the complete thermal history is read, the permanent residual stresses are predicted. A 3D geometry model is considered to represent the complete residual stress domain.

Figure 1 sets out the schematic overview of the proposed numerical procedure for calculating the non-uniform residual stresses.

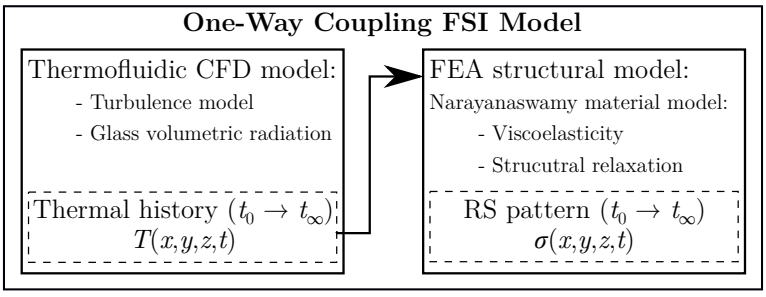

Figure 1: Flow chart of the proposed FSI one-way procedure to estimate the residual stress pattern over time. Firstly, the spatial thermal history along the tempering process is obtained by means of a thermofluidic CFD model, which computes turbulence and volumetric radiation. Secondly, the obtained thermal history is sequentially coupled to feed the mechanical model, where viscoelasticity and structural relaxation phenomena are considered for estimating the residual stress pattern.

2.1. Fundamentals

This section overviews the different mechanisms involved in the residual stress development during tempering. Firstly, residual stresses are shown to be strongly dependent on the temperature history of the material. Therefore, understanding of flow modelling and heat transfer, such as radiation in semi-transparent media, becomes a paramount matter for predicting and controlling the residual stress state of heat treated glass. Afterwards, the material constitutive model encompassing the material properties, viscoelastic stress relaxation and the structural relaxation phenomena is discussed.

2.1.1. Governing equations

The fluid phase and heat and mass transfer are modelled by the Navier-Stokes equations, composed of the conservation of mass and the momentum.

On the one hand, the continuity equation can be written in partial differential form as follows:

$$\frac{\partial \rho}{\partial t} + \nabla \cdot (\rho \vec{v}) = 0, \tag{1}$$

where ρ is the density and $\vec{v}$ is the velocity. The first term represents the mass rate increase in time and the second one the mass flow out of the control volume. On the other hand, conservation of momentum in an inertial or non-accelerating reference frame can be described in partial differential form as follows:

$$\frac{\partial (\rho \vec{v})}{\partial t} + \nabla \cdot (\rho \vec{v} \vec{v}) = -\nabla p + \rho \vec{g} + \mu \nabla^2 \vec{v} + \vec{F}. \tag{2}$$

The first term on the left side represents the momentum increase rate, and the second term the momentum flux composed of static pressure gradient, gravitational forces, the viscous stress tensor and external body forces, respectively.

Regarding heat transfer analysis, density is no longer constant and an additional fundamental equation is needed to complete the system. This relation is the energy equation given by:

$$\frac{\partial}{\partial t}\left[\rho\left(e + \frac{v^2}{2}\right)\right] + \nabla \cdot \left[\rho\left(e + \frac{v^2}{2}\right)\vec{v}\right] = \nabla \cdot (k_{\mathrm{th,f}} \nabla T + (\boldsymbol{\tau}_{\mathbf{v}} \cdot \vec{v})) - \nabla \cdot (p\vec{v}) + S_{\mathrm{h}}. \tag{3}$$

In this equation the bracketed term is the total energy of the flow composed of the internal and kinetic energies, $k_{\mathrm{th,f}}$ is the thermal conductivity of the fluid and $\boldsymbol{\tau}_{\mathbf{v}}$ the viscous stress tensor. The terms on the right-hand side of the equation represent the energy transfer due to conduction, viscous dissipation and the sources of energy S_{h}, which include the heat generation due to chemical reactions, radiation source terms or heat transfer between the continuous and a discrete phase. In the solid region, the energy equation shows the following form:

$$\frac{\partial T}{\partial t} \rho_{\mathrm{g}} c_{\mathrm{p,g}} = \nabla \cdot \left(k_{\mathrm{th,g}} \nabla T\right) + \dot{q}, \tag{4}$$

where ρ_g, $c_{p,g}$ and $k_{th,g}$ are the density, specific heat and conductivity of glass, respectively, and $\dot{q}$ is the volumetric heat generation.

2.1.2. Radiation modelling

Radiation in semi-transparent media becomes a volumetric phenomenon rather than a surface effect demanding specific modelling techniques. Gardon was the one who presented a pioneering model for calculating the temperature variation considering the volumetric feature of glass radiation [36]. The author considered the bulk radiation effect of glass, meaning that each element inside the volume of the material was able to emit and absorb energy. As a result, this process tended to homogenize the temperature within the material, while in opaque materials conduction is the only mechanism that enable this heat distribution. Recently, Siedow et al. described three main numerical methodologies to solve the complex mathematical formulation related to the radiative bulk behaviour of glass: the diffusion or Rosseland approximation, methods based on the spherical harmonic expansion (P_N approximation) and the discrete ordinates method (DOM) [37]. Among them, the DOM was considered to be the most accurate one but it also involved a high computational cost [38]. Because of this reason, many authors have neglected the volumetric feature of glass radiation in order to simplify the numerical computation [18, 17]. Other authors included the radiation effect on the defined convective HTC [12, 39]. Bernard et al. proposed an alternative solution based on two radiative fluxes by defining a surface emissivity for the opaque spectral field and a volume emissivity for the semi-transparent wavelength range, respectively [13, 14] . Nevertheless, no radiation interaction within the volume was considered. Lately, Siedow et al. and Agboka et al. performed 1D thermomechanical analysis and compared different methods for the computation of radiation in glass [33, 34]. The authors showed in terms of residual stresses that the modified DOM was in better agreement with the experimental results.

The DOM solves the radiative transfer equation (RTE) by defining a finite number of discrete solid angles. Each angle is defined by a vector direction $\vec{s}$ in the global Cartesian system (x, y, z). This method also allows to model non-grey radiation assuming a grey-band model. As glass exhibits a banded behaviour of this type, a constant spectral absorption coefficient a_λ for each wavelength band can be assumed.

The RTE for a non-grey model and in terms of spectral radiative intensity $I_\lambda(\vec{r}, \vec{s})$ can be written as:

$$\nabla \cdot (I_\lambda(\vec{r}, \vec{s})\vec{s}) + (a_\lambda + \sigma_{sc})\, I_\lambda(\vec{r}, \vec{s}) = a_\lambda I_{b,\lambda} + \frac{\sigma_{sc}}{4\pi} \int_0^{4\pi} I_\lambda(\vec{r}, \vec{s})\Phi(\vec{s}, \vec{s}')\mathrm{d}\Omega'. \tag{5}$$

In this equation $\vec{r}$ is the position vector, $\vec{s}$ is the direction vector, $\vec{s}'$ is the scattering direction vector and σ_{sc} is the scattering coefficient. The spectral absorption coefficient is denoted by a_λ and $I_{b\lambda}$ is the black body intensity given by the Planck function. Finally, the phase function and solid angle are represented as Φ and Ω', respectively.

2.2. Material model

2.2.1. Viscoelasticity

Glass is considered a linear viscoelastic material. These materials are generally modelled by phenomenological spring and dashpot models, such as the Generalized Maxwell model. This way, the time dependent linear viscoelastic behaviour of the material is delineated by means of a differential equation. In 1876 Boltzmann developed a more general model for materials exhibiting multiple relaxation mechanisms [40]:

$$\boldsymbol{\sigma_{ij}}(t) = 2\int_0^t G\left(t-t'\right)\frac{\mathrm{d}\boldsymbol{e_{ij}}\left(t'\right)}{\mathrm{d}t'}\mathrm{d}t' + \delta_{ij}\int_0^t K\left(t-t'\right)\frac{\mathrm{d}\varepsilon_{ii}\left(t'\right)}{\mathrm{d}t'}\mathrm{d}t'. \tag{6}$$

where $\boldsymbol{\sigma_{ij}}$ is the stress tensor, t refers to the time, t' is an incremental parameter for time, $\boldsymbol{e_{ij}}$ is the deviatoric strain tensor, ε_{ii} is the trace of the strain tensor and δ_{ij} is the Kronecker's delta. According to the Boltzmann superposition principle, the stress relaxation due to viscoelasticity is characterized by the time dependent shear $G(t)$ and bulk $K(t)$ modulus. The shear modulus affects to the deviatoric stress while the bulk modulus to the hydrostatic stress. These relaxation modules can be described as a series of exponential functions known as Prony series [35].

In addition to time, temperature has a strong influence on the viscoelastic material properties. The characterization of the stress relaxation curves implies a hard experimental work in order to obtain the different relaxation curves under different loads for each temperature. However, in certain cases it is possible to shift the normalized relaxation curves and build a single master relaxation curve based on a reference temperature T_B. The materials that are able to relate the time and temperature in this manner are known as thermorheological simple materials, and glass is characterized by this behaviour. For this reason, the relaxation function of glass obtained at an arbitrary temperature can be transformed to another temperature by defining a scaled time ξ instead of the real time t. The scaled time has the dimension of time and is given by the following expression:

$$\xi = \phi(T)t. \tag{7}$$

The shift function, $\phi(T)$, which is generally used to scale the real time t, obeys an Arrehnius type law:

$$\ln\phi(T) = \ln\frac{\mu_\mathrm{g}\left(T_\mathrm{B}\right)}{\mu_\mathrm{g}(T)} = \frac{H}{\mathrm{R_g}}\left(\frac{1}{T_\mathrm{B}} - \frac{1}{T}\right), \tag{8}$$

where μ_g is the dynamic viscosity of glass, T is an arbitrary temperature, T_B the reference temperature, H is the activation energy and $\mathrm{R_g}$ is the universal gas constant.

2.2.2. Structural relaxation

Depending on the rate of heating or cooling, certain glass properties such as density are varied. This fact occurs due to the structural arrangement of the atoms. In addition, the structural relaxation is deemed as an influential phenomenon during the residual stress development in glass [9]. Based on the mathematical formulation proposed

by Narayanaswamy [8], Figure 2 shows the volumetric contraction phenomena over the glass transition range. As can be observed, the volumetric contraction varied not only with temperature but also with the applied cooling rate, whereas the thermal contraction remained constant. All the same, it always shows the same shape; it increases with temperature and stabilizes beyond the glass transition temperature, T_g .

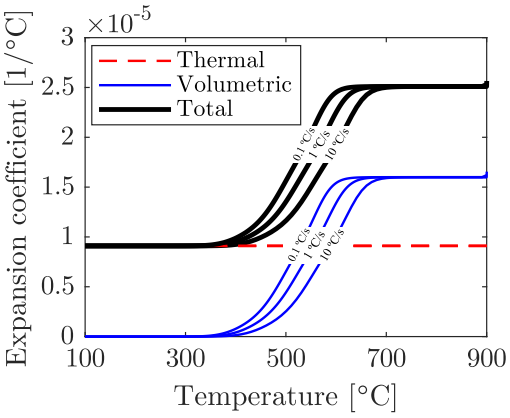

Figure 2: Variation of thermal and volumetric expansion coefficients over the glass transition range for different cooling rates: 0.1 °C/s, 1 °C/s and 10 °C/s. The volumetric contribution to the total contraction coefficient vanishes at a higher temperature with increasing cooling rate.

When a low cooling rate was applied, such as 0.01 °C/s, the contribution of the volumetric expansion coefficient vanished at 350 °C, whereas if a higher cooling rate was applied, namely, 10 °C/s, this phenomenon occurred at 400 °C. The latter case had more to do with the cooling rate magnitude that normally occurs during the tempering process. Similarly, Figure 3 sets out the variation of normalised volume over the glass transition range when the material is subjected to different cooling rates. As shown here, the higher the applied cooling rate, the higher the volume in the material. As a result, the density of the material became smaller for high cooling rate processes than for a lower cooling rate process. This fact combined with a non-uniform cooling leads to a non-uniform contraction of the material, which might be considered as the main source of residual stresses. Additionally, it is possible to observe that almost all the structural arrangement occurred in the glass transition range. However, as glass is an amorphous material, its microstructure continued to rearrange even at lower temperatures.

With the aim of describing the microstructural state of glass, Tool introduced the concept of fictive temperature, T_f, as a measure of the degree of non-equilibrium glass [41]. In 1971 Narayanaswamy proposed a structural model that accounted for these cooling rate dependent properties [8]. In this regard, a new mathematical statement for determining the fictive temperature was presented. This way, the fictive temperature was observed to be dependent on the response function $M_p(t)$, which is obtained experimentally:

$$T_f(t) = T(t) - \int_0^t M_p\left(\xi(t) - \xi'(t)\right) \frac{\partial T\left(t'\right)}{\partial t'} \mathrm{d}t. \tag{9}$$

When the fictive temperature was found, the thermal strains could be calculated by the next equation:

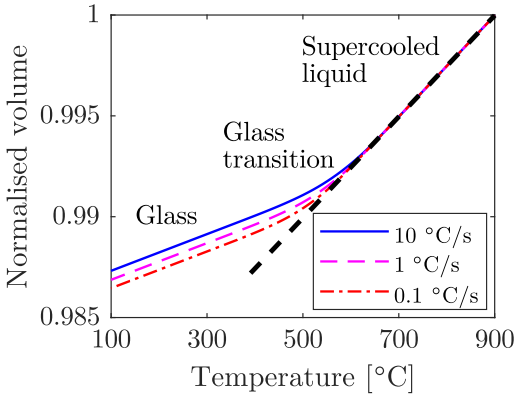

Figure 3: Variation of normalised volume over the glass transition range for different cooling rates: 0.1 °C/s, 1 °C/s and 10 °C/s. The change in rate of volume contraction occured at a higher temperature with increasing cooling rate.

$$\Delta\varepsilon_{ij}^{\mathrm{th}} = \delta_{ij}\Delta\varepsilon_{\mathrm{th}} = \delta_{ij}\left(\alpha_{\mathrm{g}}\Delta T + \left(\alpha_{\mathrm{l}} - \alpha_{\mathrm{g}}\right)\Delta T_{\mathrm{f}}\right), \tag{10}$$

where δ_{ij} is the Kronecker delta and α_{l} and α_{g} are the thermal expansion coefficients for the liquid and solid state, respectively.

2.3. Computational cost reduction techniques

The present FSI one-way procedure involves a large computational cost mainly due to the radiation phenomenon and the fluid flow computation. Thermal radiation in semi-transparent media gains special relevance, as it becomes a volumetric phenomenon as compared to opaque materials. Nevertheless, it also involves a large computational cost as it depends on many parameters, such as; direction, wavelength, time, thickness of the material, and so forth. According to some authors however, the importance of radiation decreased for low thickness and high cooling rates [33, 42]. Therefore, when low thickness and high cooling rates are combined, radiation might be neglected in order to reduce the computational cost of the model.

In addition to radiation phenomenon, CFD simulations usually imply the use of small time increments, as low as milliseconds, to solve the physics related to turbulence and heat transfer. Consequently, the proposed FSI procedure involves a large computational cost and needs a high amount of computational resources making it unfeasible for an industrial time scale. For this reason, with the aim of further decreasing the computational cost, the mechanisms involved on the residual stress development needed to be understood.

The structural relaxation of glass is known as an important source of residual stresses during the glass cooling process [9]. As shown in Figure 2 however, taking into account the cooling rate magnitudes that are normally involved in the tempering process, the volumetric feature of glass expansion vanished at 400 °C. At this point, glass is well below the T_{g} and behaves as an elastic solid material, making the volumetric expansion to lose traction. As a result, there might be a critical time, t_{cri}, with its associated critical temperature, where residual stresses are no longer

influenced by cooling rate and become independent of thermal history.

Additionally, an alternative for further reduce the computational cost was reported in the literature [19]. This approach simplified the transient calculation of the flow by defining a spatially non-uniform but time constant HTC distribution.

With the view to validating these assumptions and optimizing the current FSI one-way procedure for quenching modelling, the influence of each computational cost reduction technique in the final residual stress pattern was evaluated. From this assessment, the following main conclusions were drawn:

- Firstly, the influence of volumetric radiation was found to be negligible when low thickness components were subjected to large heat extractions.
- Secondly, the existence of a critical temperature below which the obtained residual stress pattern was independent from the applied cooling rate was verified.
- Finally, it was found that the use of spatially non-uniform steady HTC could be a cost-effective solution but it could also present some limitations regarding the residual stress pattern when complex transient flow phenomena became of relevance.

Based on this conclusions, the proposed modified procedure to model low thickness quenching processes encompasses both, a transient CFD simulation without volumetric radiation and a purely thermal model below the critical temperature. This way, a commitment between accuracy and efficiency was sought. The use of a steady HTC could be an additional implementation but the flow nature and its influence should be first addressed. In this regard, Figure 4 presents the computational sequence of the proposed modified procedure.

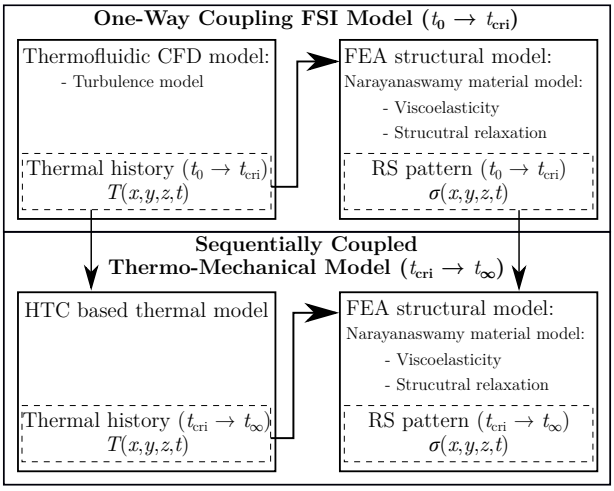

Figure 4: Flow chart of the proposed modified procedure to estimate the residual stress pattern over time. The procedure is divided into two stages: firstly, a FSI one-way approach is adopted to consider the local heat exchange at the onset of cooling until the critical temperature instant (t_{cri}) is attained. Subsequently, a sequentially coupled thermo-mechanical approach based on a uniform HTC is proposed from t_{cri} to steady-state temperature instant (t_∞) for obtaining the final residual stress pattern.

As presented in Figure 4, a CFD model without volumetric radiation was defined with the aim of capturing the transient local flow phenomena during the initial stage of the cooling process. However, once the highest temperature in the model was below 400 °C, namely, when the critical time was reached, the CFD calculation was interrupted. At this point, the obtained initial thermal history was transferred to a thermal model where a constant in time and spatially uniform HTC was applied. Here, the remaining thermal history until room temperature was calculated. Finally, the complete thermal history was read into the structural model and the non-uniform residual stresses were predicted.

3. Application to tempering of glass plates

This section firstly introduces the experimental work used for validating the proposed numerical procedure. Subsequently, a mesh sensitivity analysis is performed and the numerical model is delineated. When the numerical model and grid are established, the different computational cost reduction techniques are assessed. More specifically, the influence of volumetric radiation on the non-uniform residual stress distribution of tempered glass plates, the existence of a critical temperature and the influence of considering a spatially non-uniform steady HTC are investigated. Finally, the validation of the proposed procedure with respect to the FSI one-way procedure, which considers the volumetric radiation phenomenon and shows no interruption of the CFD calculation during the cooling process, is done.

3.1. Experimental study from the literature

The analysed case study alluded to the work presented by Chen et al. where they measured the residual stress distribution after tempering flat glass specimens of 6 mm thickness [23]. Even though the specimens had a dimension of 300 x 300 x 6 mm, the analysis of the results was limited to a representative area of 28 x 56 mm composed by a centred and its four neighbouring jets (see Figure 5).

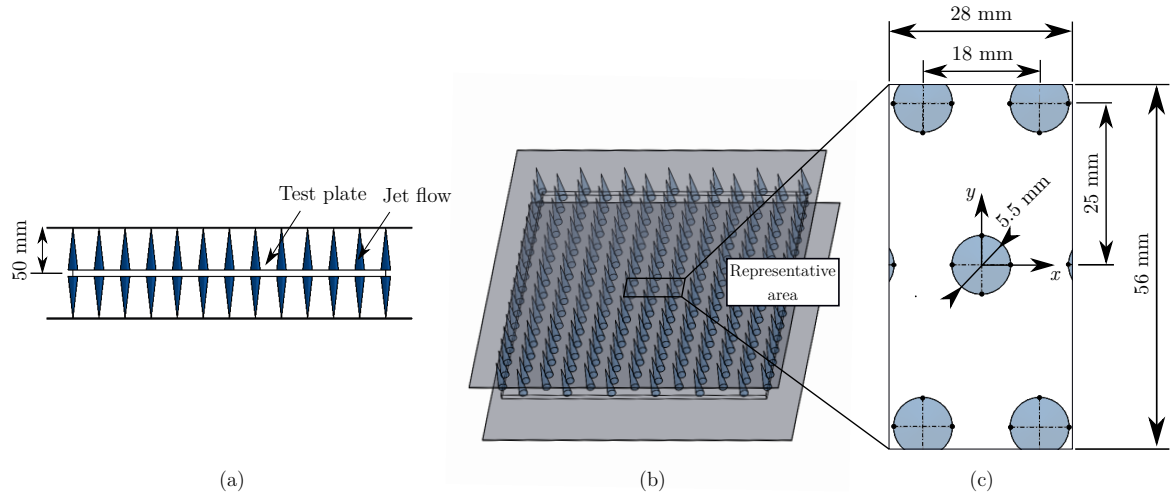

Figure 5: Schematic representation of the cooling unit over the glass plate and the area of interest: (a) side view; (b) isometric view; and (c) detail of the area of interest.

The cooling jets consisted of a perforated plate with 5.5 mm diameter holes. The distance between adjacent jet columns and rows were 18 mm and 25 mm, respectively. Regarding the nozzle-to-plate distance, it was defined at 50 mm. Finally, the glass sample was symmetrically cooled from both sides.

3.2. Numerical model

Next, the main features of the model, the defined boundary conditions and the material constitutive model are delineated.

3.2.1. Fluidic computational domain

Figure 6 presents the computational domain composed of the glass plate and the fluid domain. The nozzle arrangement and its dimensions, as well as the process parameters were based on the work of Chen et al. [23]. For reducing the computational time, a $1/8^{\text{th}}$ model was defined by the use of three symmetry planes. Likewise, the computational grid was extended sufficiently far to the sides in order to led the nozzle array flow to develop before reaching the outlet boundary condition.

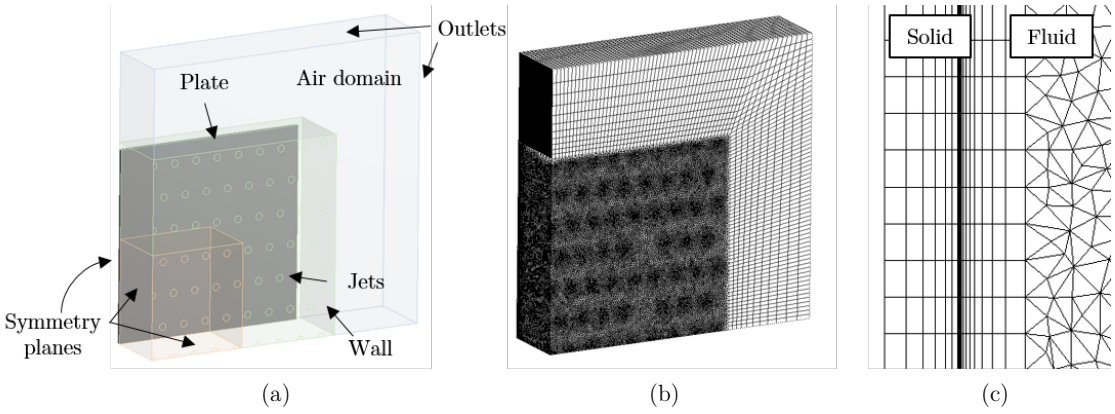

Figure 6: Three dimensional symmetric model used in the numerical calculation: (a) $1/8^{\text{th}}$ symmetry computational domain; (b) mesh discretization; and (c) detail of the near wall mesh.

The central fluid region in contact with the glass plate was discretized with a finer mesh than the surrounding fluid volume in order to make the calculation more efficient. Six hexahedral elements were defined through half the thickness of the plate and a bias factor of four was used to better capture the thermal gradients developed on the surface. Tetrahedrons were used for meshing the air volume and 14 inflation layers with a first layer thickness of 10 μm were defined near the glass wall to obtain a wall y^+ value in the order of unity. This y^+ value is the recommended one for correctly modelling the boundary layer when the $k-\omega$ turbulence model is used.

The $k-\omega$ turbulence model has gained popularity as it is considered to be more accurate than $k-\epsilon$ models for boundary layer flows [43]. Particularly this is the case for the Shear Stress Transport (SST) model. The SST model is a two equation turbulent model where the $k-\omega$ model is employed for solving the boundary layer and the $k-\epsilon$ model is used to solve the freestream flow in the far field. Additionally, Zuckerman & Lior performed an

exhaustive review about turbulence modelling and considered the SST model as one of the most appropriate options for modelling impinging jets in terms of accuracy and computational cost [27]. Recently however, ANSYS developed a new turbulence model family called Generalized $k-\omega$ (GEKO) model. GEKO is based on the $k-\omega$ model formulation, but with the flexibility to cover a wide range of flow scenarios, such as jet impingement. This way, a better prediction of the round jet expansion is achieved, as conventional models like SST may overpredict the spreading rate of round jets substantially. Similarly, the Intermittency Transition model with Kato-Launder production limiter was considered as it deals with the overprediction of the heat transfer in the stagnation zones [44]. This option limits the excessive production of turbulence kinetic energy caused by a high level of shear stress rate in the stagnation regions.

Regarding the solver, a pressure-based solver was employed as the defined flows were subsonic. The SIMPLE algorithm was used to solve the pressure and velocity fields and the second order upwind scheme was selected as interpolation method. The convergence criterion was defined based on the root mean square residuals of each equation. On the one hand, a value below 10^{-4} was considered for the momentum, mass, and turbulent equations, whereas a value below 10^{-6} was defined for the energy and radiation calculations.

Circular inlet conditions referring to each jet were defined. Here, uniform velocity boundary conditions were imposed while pressure outlet boundary conditions were defined at the outflow boundaries. The air flow velocity was defined at 100 m/s and 200 m/s as stated in the experimental work in literature.

The DOM was used for considering the volumetric radiation phenomenon in the glass plate. This way, a grey-banded behaviour was assumed for the absorption coefficient. With the view to clarifying the influence of volumetric radiation on the residual stress distribution during the glass tempering process, calculations were made with and without considering radiation.

3.2.2. Structural computational domain

After performing the CFD calculation, a structural analysis was performed by importing the model into the finite element software. The same symmetry conditions and mesh as in the fluidic calculation were used. However, in this case the fluid domain was removed and the numerical model was only composed of the solid glass plate. According to the element type, quadratic full-integration hexahedral elements were defined. The mesh consisted of 60000 elements, being composed of six elements through half the thickness.

3.2.3. Material properties

Glass was modelled by the constitutive model described by Narayanaswamy, which accounted for the viscoelasticity and structural relaxation phenomena [8]. For this reason, a user-defined subroutine UMAT was used to account for the high temperature behaviour of glass. In the present study, the UMAT was built based on the valuable contribution of Nielsen, who presented and validated the model of Narayanaswamy for the glass tempering process in a commercial Finite Element code [35]. Similarly, the material parameters for the exponential series used for viscoelasticity and for the structural response function were based on the data described in the study of Nielsen [39].

The temperature dependent thermal conductivity and specific heat for soda-lime glass were based on data from the literature [12]:

$$k_{\mathrm{th,g}} = 0.741 + 8.58 \cdot 10^{-4} T, \tag{11}$$

$$c_{\mathrm{p,g}} = \begin{cases} 1433 + 6.5 \cdot 10^{-3} T & T \geq 850 \text{ K} \\ 893 + 0.4T - 18 \cdot 10^{-8} T^{-2} & T < 850 \text{ K}. \end{cases} \tag{12}$$

Regarding the physical properties, a density of 2470 kg/m^3 for soda-lime glass was defined. In addition to these properties, a grey banded behaviour was assumed for modelling the absorption coefficient. Table 1 provides the defined absorption coefficient values for each wavelength range, whereas the refractive index was assumed to remain constant at 1.5 for the analysed region of the spectrum based on the work of Nicolau & Maluf [45].

Table 1: Absorption coefficient values for specified wavelength bands.

Wavelength [μm]	**Absorption coefficient [1/m]**
0.4 - 1.4	150
1.4 - 2.9	90
2.9 - 4	390

The absorption coefficient strongly increased after 2.9 μm, meaning that glass became opaque for long wave radiation. With regard to the thermal properties of the cooling fluid, temperature dependent properties of air at ambient pressure were considered [46]. The specific heat, thermal conductivity and dynamic viscosity were defined as a function of temperature, whereas the ideal gas law was used to calculate the density of the air.

3.3. Post-processing procedure

In this section, the followed post-processing procedure is summarised. With the aim of reducing the computational cost, a 1/8$^{\mathrm{th}}$ symmetry domain was modelled. As presented in Figure 7, the result discussion was limited to the largest stress gradient area, composed by a centred and its four neighbouring jets. This analysis area was also the one defined by previous experimental investigations for measuring the residual stress magnitude on the surface of the components [23]. Therefore, the obtained residual stress results were restricted to this area.

Once the analysis area was defined, the following post-processing features were proposed for analysing the results:

- Absolute maximum principal stress contour plots in the area of analysis were shown in order to identify the tensile and compressive regions.
- Two control points located in the dry region, $\mathrm{P_{dry}}$, and jet facing area, $\mathrm{P_{jet}}$, were considered for analysing the residual stress variation over time on both, the surface, $(\bullet)_{\mathrm{s}}$ and on the core, $(\bullet)_{\mathrm{c}}$, of the component. The dry region refers to the area between jets, $(\bullet)_{\mathrm{dry}}$, whereas the jet region to the stagnation or jet facing area $(\bullet)_{\mathrm{jet}}$.

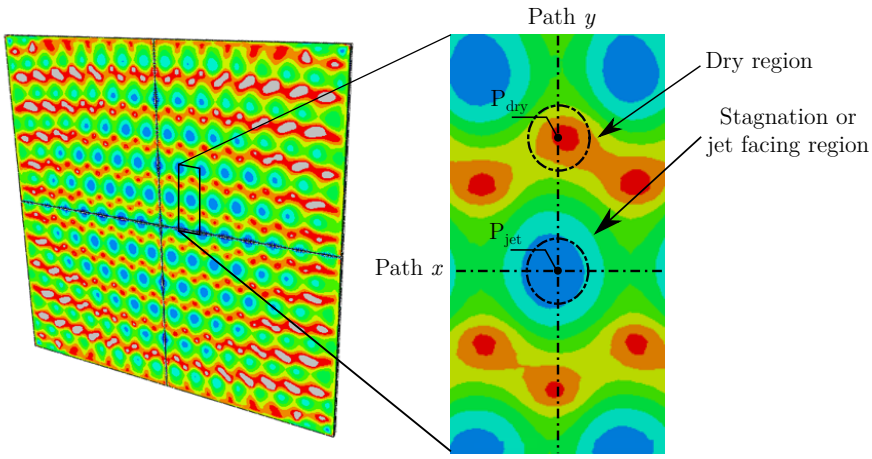

Figure 7: Absolute maximum principal stress pattern on the complete glass surface and the area of interest, where the jet and dry regions and the x and y paths for performing subsequent experimental validations are defined.

- Two paths along the x and y directions were defined to validate the obtained residual stress magnitudes against experimental measurements.

3.4. Mesh sensitivity analysis

Firstly, a mesh sensitivity analysis was performed to assess the quality of the numerical results. For this reason, the size and density of the grid cells related to the air domain were varied until mesh independent results were achieved. Element sizes of 2.25, 1.5 and 1.125 mm for the plate and air domain were defined. As a result, a coarse mesh made out of 960935 elements (mesh 1), an intermediate mesh of 3,671,976 (mesh 2) and a fine mesh of 4,851,349 (mesh 3) were studied.

Figure 8 compares the residual stress variation over time on the surface and core of the jet and dry regions, when cooling a glass plate by a 100 m/s air flow. As the ordinary residual stress state defined by σ_{x} and σ_{y} depends on the directional feature of the selected coordinate system, the absolute maximum principal stresses were used for the term residual stress.

The coarser grid showed a deviation up to 20%, whereas a deviation of 4% was obtained comparing the finer meshes. Hence, the grid configuration with 3,671,976 cells was selected for the following calculations.

3.5. Assessment of computational cost reduction techniques

Hereafter, the analysed computational cost reduction techniques are investigated, namely, the influence of volumetric radiation, the existence of a critical temperature and the influence of assuming a spatially non-uniform time-constant HTC distribution during the tempering process.

3.5.1. Volumetric radiation influence

Firstly, the influence of volumetric radiation on the residual stress development was checked. Even if the initial temperature distribution of the plate after the heating process might play an important role on the residual stress devel-

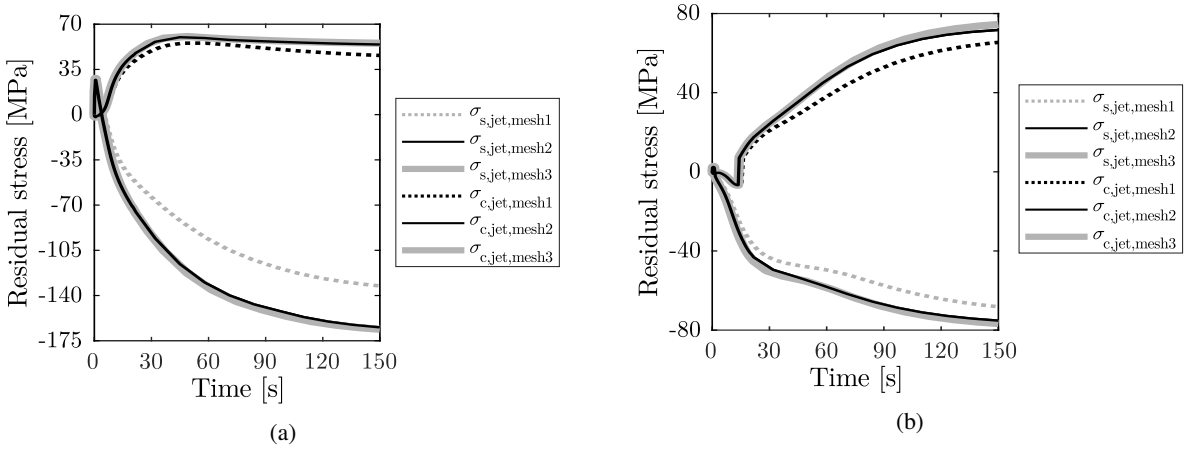

Figure 8: Influence of mesh refinement on the absolute maximum principal stress variation over time on the surface and the core of the glass plate in the: (a) jet facing area; (b) dry region.

opment, due to the lack of information regarding the thermal history of the components, a uniform initial temperature of 650 °C was assumed. Figure 9 sets out the numerically calculated residual stress patterns corresponding to an air velocity of 100 m/s and 200 m/s at the cooling jet exit considering and neglecting the radiation phenomenon. The proposed jet velocities were defined according to the experimental work in literature [23].

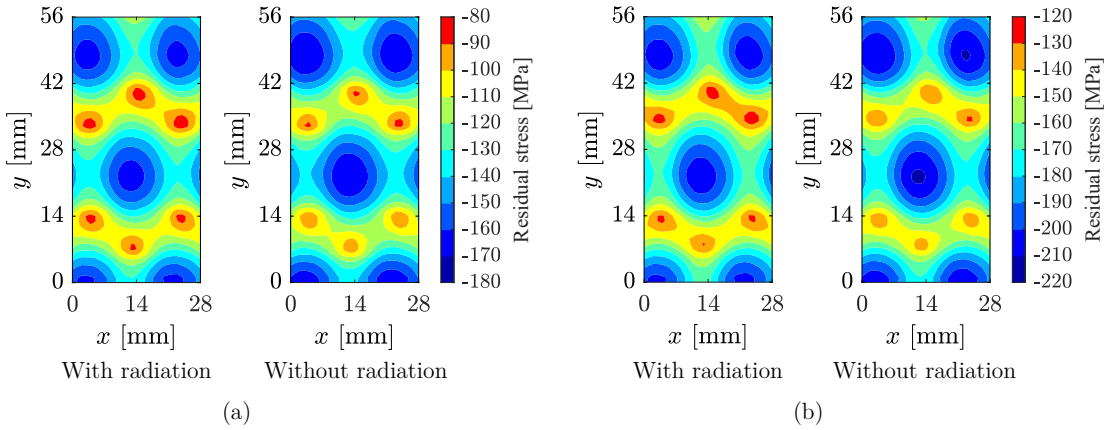

Figure 9: Volumetric radiation influence on the estimated surface residual stresses for both analysed jet velocities: (a) v = 100 m/s; (b) v = 200 m/s.

The observed large stress variations arose due to the lack of horizontal movement of the plate during the cooling down process [23]. Similarly, higher compressive stresses were observed in the locations where the cooling jets were defined. This fact might be explained by the different thermal gradients developed in the plate. Figure 10 sets out the temperature difference between the surface and the core of the jet facing area and dry region.

At first instance, the surface cooled more rapidly because of the intense jet convection. Nevertheless, the low conductivity of glass hindered a rapid response of the core leading to a large temperature difference at the beginning of the process. The difference increased until a maximum was reached. This maximum point referred to the onset of

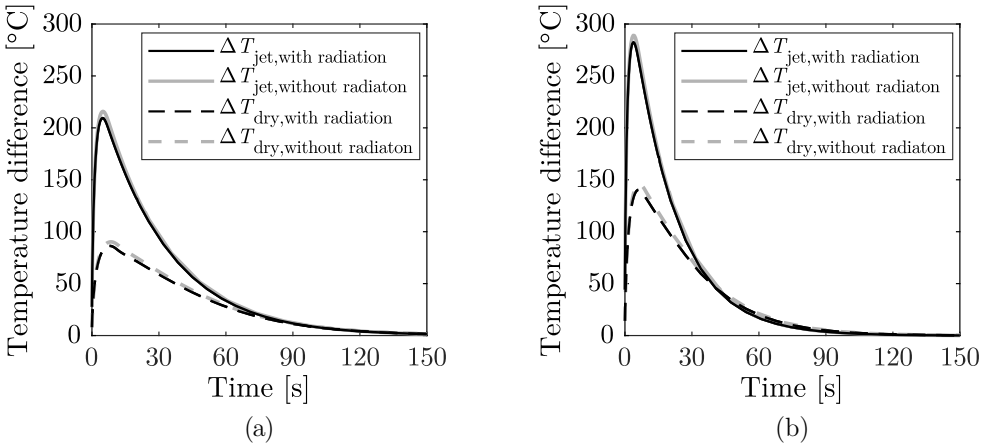

Figure 10: Volumetric radiation influence on the temperature difference between the surface and the core of the plate in the jet facing and dry regions for both analysed air velocities: (a) v = 100 m/s; (b) v = 200 m/s.

cooling of the core. A maximum difference of 210 °C was reached in the jet facing area and 85 °C in the dry regions for the 100 m/s air flow, whereas 280 °C and 140 °C were reached for the 200 m/s air flow. As a result, the heat extraction was significantly larger in the stagnation area of the jet than on the outer regions, which gave rise to the generation of hot spots in the areas between jets, the so-called dry regions. This fact resulted in a non-homogeneous temperature distribution on the surface of the plate, which seems to be directly related to the non-uniform nature of the residual stress distribution during air jet cooling.

The influence of volumetric radiation on the final residual stress distribution for a certain jet velocity is low, as residual stresses shared a similar pattern (see Figure 9). In the case of 100 m/s air flow, the final residual stress magnitudes differed up to 3% in the jet facing area and 5% in the dry region. The most striking result to emerge from this data is that as cooling rate increases, the influence of radiation became smaller as these differences decreased down to 2% and 4% with an air velocity of 200 m/s. Figure 11 provides a deeper insight by comparing the effect of radiation on the stress prediction along the x and y directions.

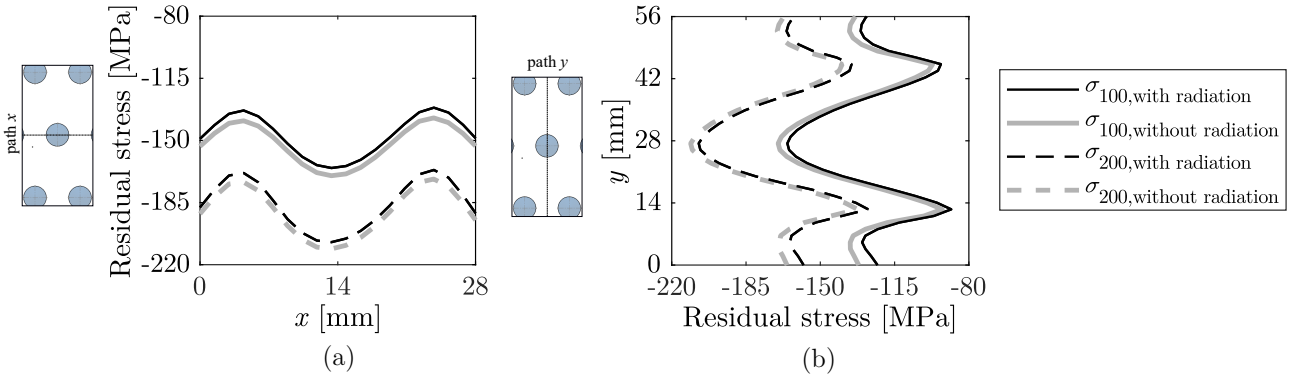

Figure 11: Influence of volumetric radiation on the distribution of absolute maximum principal stresses on the surface of the plate when subjected to 100 m/s and 200 m/s air flows. The stress distribution is shown along: (a) path x; (b) path y.

Interestingly, the influence of radiation resulted in a decrease of residual stresses by offsetting its magnitude along the *x* and *y* directions. This decrease however, might be considered as negligible as it remained below 5% for both analysed flows. The reason for this may rely on the short period of time that the components remained at high temperature. The contribution of radiation to the total heat transfer rate showed a maximum of 6% and 4% at the beginning of the cooling process for an air velocity of 100 m/s and 200 m/s, respectively. Additionally, once these maximums were reached, they decreased as temperature did so as can be seen in Figure 12.

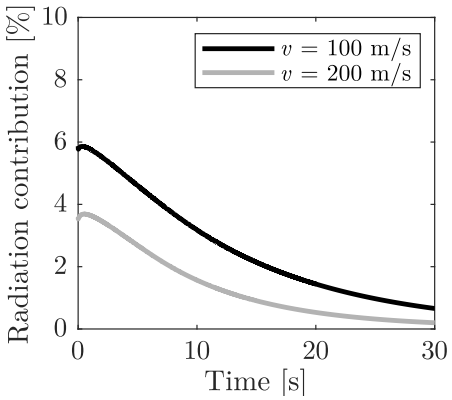

Figure 12: Contribution of radiation to the total heat transfer rate during air jet cooling by 100 m/s and 200 m/s.

Consequently, as the air jet velocity was increased, the cooling rate increased and the effect of radiation on the residual stress pattern became lower. Overall, the obtained residual stress distribution considering and without considering radiation showed a huge similarity. The evidence shown here became also reasonable for any plate thickness up to 6 mm. As radiation losses relevance with increasing cooling rate or decreasing thickness, values lower than 6 mm are bound to lead to similar conclusions. For thicker components though, volumetric radiation might play a relevant role on the thermal distribution within the material and a more thorough analysis may be required. Notwithstanding, this was a remarkable outcome regarding the main drawback of the FSI one-way procedure, namely, the computational cost. Taking into account the small differences observed on the final residual stress pattern, radiation might be neglected when low thickness glassware is subjected to large heat extractions, such as in the tempering process.

3.5.2. Existence of a critical temperature

With the aim of finding the critical temperature, where residual stresses are no longer influenced by the cooling rate, the computational sequence presented in Figure 4 was adopted. Volumetric radiation was shown to have little influence on the residual stress magnitude and distribution, and hence, it was not considered within this analysis.

The CFD calculation was performed until the hottest point, namely the core in the dry region, was at 400 °C. Thus, transient and spatially non-uniform HTCs were considered during the first stage of the cooling process. Once the critical temperature instant was reached, the fluidic and thermal computation could be interrupted and a purely thermal calculation based on a spatially uniform and constant in time HTC was performed. Thereby, different HTC resembling

natural and forced convections were defined in order to verify the cooling rate independence, more specifically, 20 W/m^{2}K, 500 W/m^{2}K and 1000 W/m^{2}K.

Figure 13 provides the residual stress distribution when the CFD calculation was interrupted at a core temperature of 400 °C and subsequently, different uniform and constant HTC were applied. Similarly, the residual stress distribution obtained by the FSI one-way procedure without considering radiation is presented.

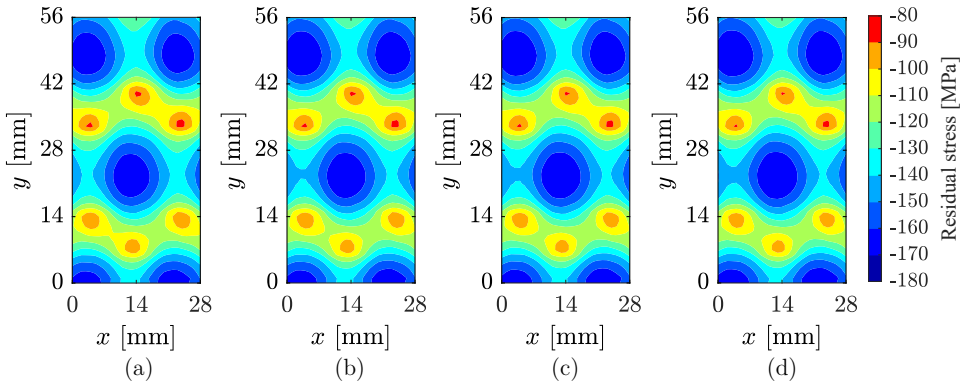

Figure 13: Estimated surface residual stress pattern for a 100 m/s air flow based on: (a) the FSI one-way procedure without considering radiation, where the spatial thermal history along the tempering process is obtained by means of a thermofluidic CFD model; and (b)-(d) the proposed procedure based on CFD analysis until a critical temperature of 400 °C is achieved, followed then by a thermo-mechanical calculation considering different HTC values: (b) h = 20 W/m^{2}K; (c) h = 500 W/m^{2}K; (d) h = 1000 W/m^{2}K.

Despite the HTC variation from 20 to 1000 W/m^{2}K, the obtained final residual stress distribution did not vary with respect to the reference case as the maximum difference remained below 2%. The most interesting aspect of these results was that the same residual stress magnitude and distribution was obtained even if each case showed a different thermal history and residual stress variation over time. This is observed in Figure 14, where the first 150 s of the cooling process are shown.

The reason for this relied on the temperature of the plate. The development of residual stresses mainly occurred due to the volumetric expansion of glass. Nevertheless, when the hottest point of the plate was at 400 °C, the critical temperature was reached and the contribution of volumetric expansion phenomenon was almost completely vanished. As a result, the subsequent cooling technique was no longer influential on the residual stress development and it became cooling rate independent within the range from natural to forced convection cooling. If the critical temperature was not reached though, residual stresses became cooling rate dependent and its final magnitude and distribution varied as a function of the adopted cooling technique. Overall, a residual stress deviation below 2% with regard to the reference model was obtained. Regarding the case of 200 m/s air flow, the same conclusions were drawn.

What stands out from this analysis is the large computational cost that radiation implied on the total calculation time. This unique assumption led to a reduction of 75% of the total computational time. Furthermore, if the CFD calculation was interrupted, an additional saving of 50% was obtained, which brought about a total decline around 87% of the computational time in respect to the initially proposed procedure.

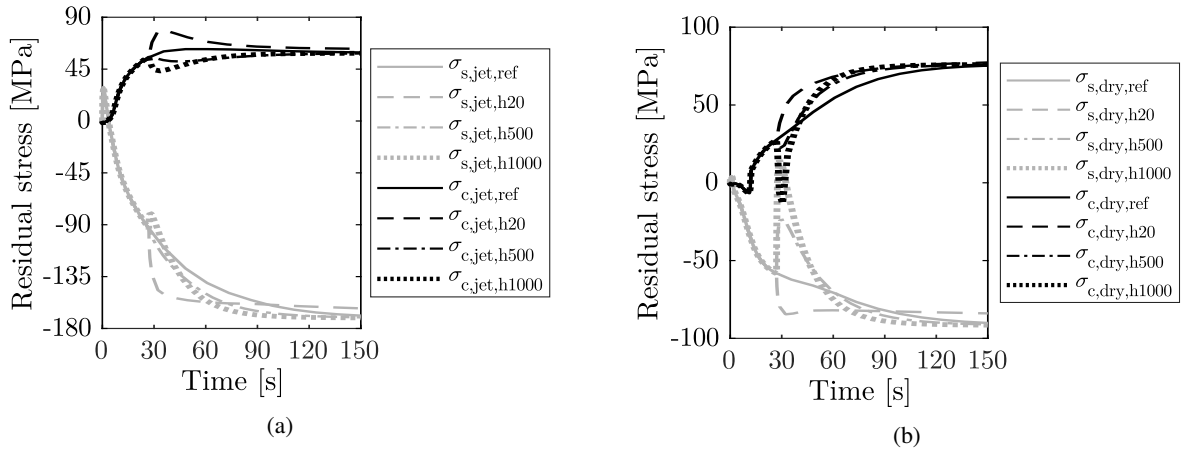

Figure 14: Variation of absolute maximum principal stresses over time on the surface and the core of the plate in the: (a) jet facing area; and (b) dry region. Results are shown for a 100 m/s air flow and the calculation is based on the proposed procedure, which relied on different HTC values: h = 20 W/m^{2}K, h = 500 W/m^{2}K, h = 1000 W/m^{2}K.

3.5.3. Spatially non-uniform steady HTC

Ultimately, the consideration of time-constant but spatially different HTC distributions for calculating residual stresses was analysed. This approximation could lead to a further reduction of the calculation time, as a steady HTC distribution could replace the transient calculation and its associated larger computational cost.

Figure 15 highlights the variation of the HTC distribution over time for a 100 m/s air flow until the maximum temperature of the plate was below 400 °C. At this instant, the critical time was reached, being in this case t_{cri} = 25 s. This way, the variation of transient and steady HTCs over time in the control points P_{jet} and P_{dry}, which are illustrated in Figure 7, were monitored.

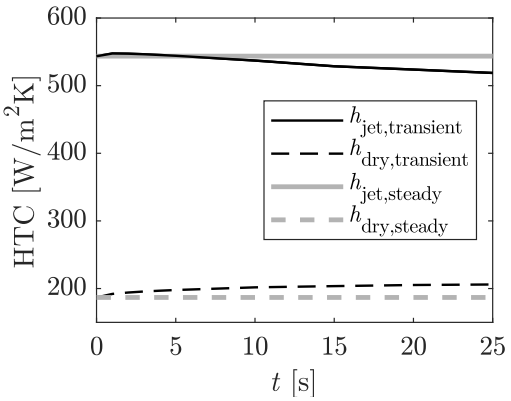

Figure 15: HTC magnitude as a function of time in the jet facing and dry regions considering transient and steady HTC.

The HTC magnitude in the stagnation point tended to decrease as time went by, whereas the one in the dry region increased as compared to a steady HTC distribution. With the aim of discussing this fact, the time-constant and transient HTC distributions on the representative analysed area were compared. For the transient calculation, the

HTC distribution referring to the critical time instant was adopted. Figure 16 shows the steady and transient HTC distributions on the quenched plate and the deviation between both approaches.

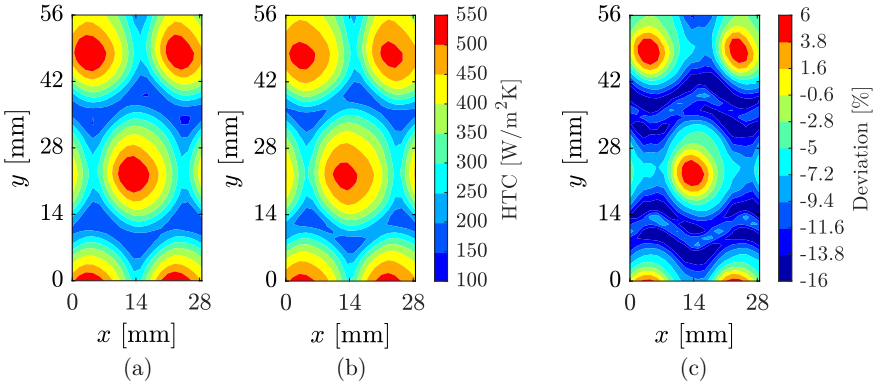

Figure 16: HTC distribution at t_{cri} instant ($t = 25s$): (a) steady HTC; (b) transient HTC; (c) deviation.

When a spatially different and time-constant HTC distribution was adopted, differences up to 16% in the dry regions were appreciated. Contrarily, differences up to 6% in the stagnation areas were observed. With regard to residual stresses, Figure 17 presents the final residual stress results in the area of interest.

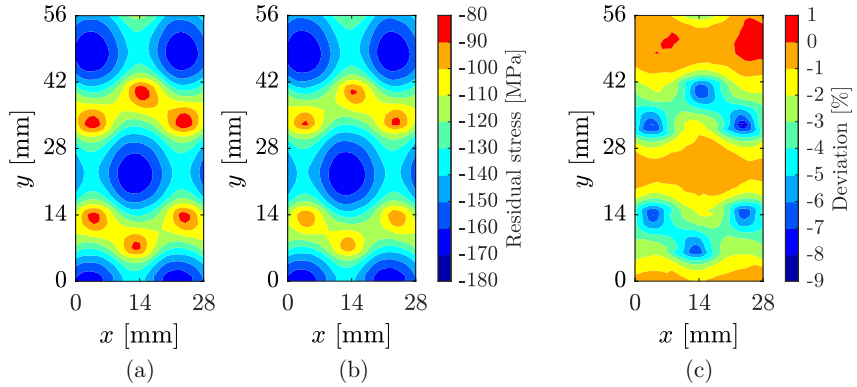

Figure 17: Final residual stress distribution on the surface: (a) based on steady HTC; (b) based on transient HTC; (c) deviation.

Differences up to 1% in the stagnation area and up to 9% in the dry region were found. Similar to the HTC distribution analysis, larger variations were observed in the dry regions. Thus, the residual stress behaviour concurred with the one shown by the HTC.

Furthermore, widening the current analysis to a $1/8^{th}$ of the geometry, a deeper insight into the obtained results was given. In this case, a $1/8^{th}$ representation of the model enabled the view of the edges of the plate, making it easier to notice the main differences between these two analysed approaches. Figure 18 includes the contour plots of the HTC on a $1/8^{th}$ of the geometry at t_{cri} instant. In the same manner, the deviation contour plot is shown.

HTC deviations up to 25% were observed in the dry regions while lower deviations up to 6% were observed in stagnation points. In addition, crossflow effects were appreciated close to the flow evacuation areas. This phenomenon

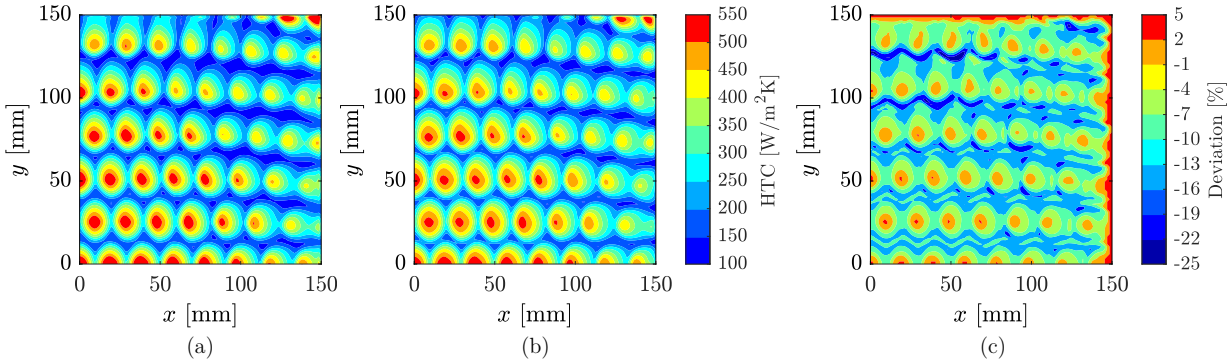

Figure 18: HTC distribution on the surface at t_{cri} instant ($t = 25s$): (a) steady HTC; (b) transient HTC; (c) deviation.

distorted the jet pattern on the glass surface and tended to increase the deviations towards the edges of the plate. With regard to residual stresses, Figure 19 provides the final residual stress pattern on the $1/8^{th}$ representation of the model considering steady HTC, transient HTC and the residual stress deviation between both approaches.

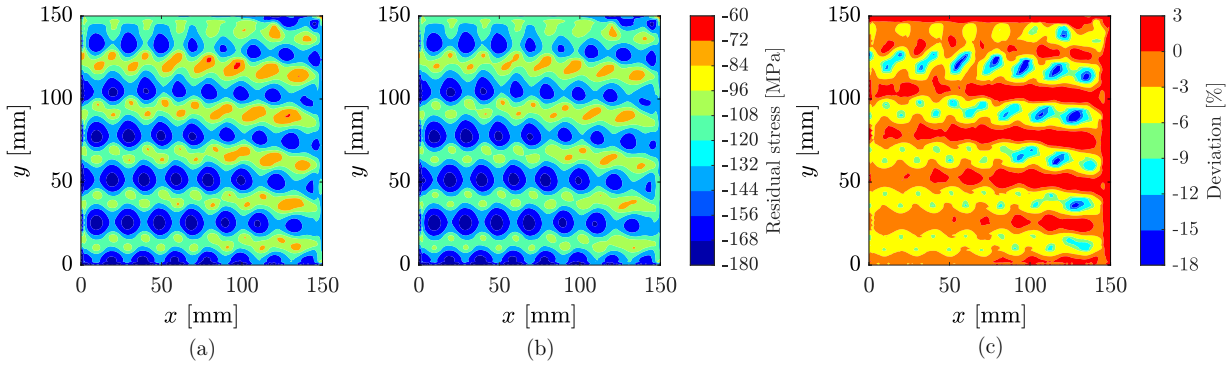

Figure 19: Final residual stress distribution on the surface: (a) based on steady HTC; (b) based on transient HTC; (c) deviation.

Deviations in residual stresses up to 3% and 17% were perceived in the jet facing and dry regions, respectively. Thus, as in the above-mentioned HTC analysis, higher deviations were observed in the dry regions. Correspondingly, differences tended to increase towards the edges of the plate due to the effect of crossflow.

The results in this section indicate that both approaches showed low differences in the stagnation points of the nozzle array. However, higher differences in the HTC and residual stress patterns were observed in the dry regions. Thus, even if the air speed through the perforated metal sheet was constant, due to the large temperature drop of the plate during the tempering process, a variation of the temperature difference between the target surface and the impinging air over time also occurred. Consequently, the thermophysical properties of air also varied having a direct impact on the interacting jet flow regime and the resultant convective HTC.

In summary, based on the conclusions drawn from the analysis of the considered computational cost reduction techniques, a modified procedure to model low thickness quenching processes was proposed. The procedure encompasses both, a CFD model without volumetric radiation to capture the transient local flow phenomena until the critical

temperature is attained, and a thermal model where a constant in time and spatially uniform HTC is applied.

4. Residual stress prediction and validation of the modified procedure

This section moves on to validate the proposed modified procedure. Nonetheless, no initial temperature specification was made on the experimental work from the literature. Previous research findings into the initial quenching temperature showed its large influence on the residual stress development. Narayanaswamy showed that for a specific cooling rate, as the initial quenching temperature was increased, the achievable degree of temper increased until a plateau was reached [9]. A similar conclusion was obtained in this aspect by Aronen & Karvinen and Agboka et al., who showed that as initial temperature increased, the maximum surface tensile stresses developed at the onset of cooling decreased for different glass thicknesses [34, 26]. In this regard, a sensitivity analysis varying the initial temperature from 600 to 650 °C was performed.

Turning now to the experimental measurements, Chen et al. measured the final residual stress distributions by SCALP, which shows an experimental uncertainty of 5% [23]. Because of this reason, the performed validation regards to the final residual stress distribution developed on the glass surface. Figure 20 sets out the experimental measurements and predicted residual stress distribution for varying initial temperatures along the *x* and *y* axes for a jet velocity of 100 m/s and 200 m/s.

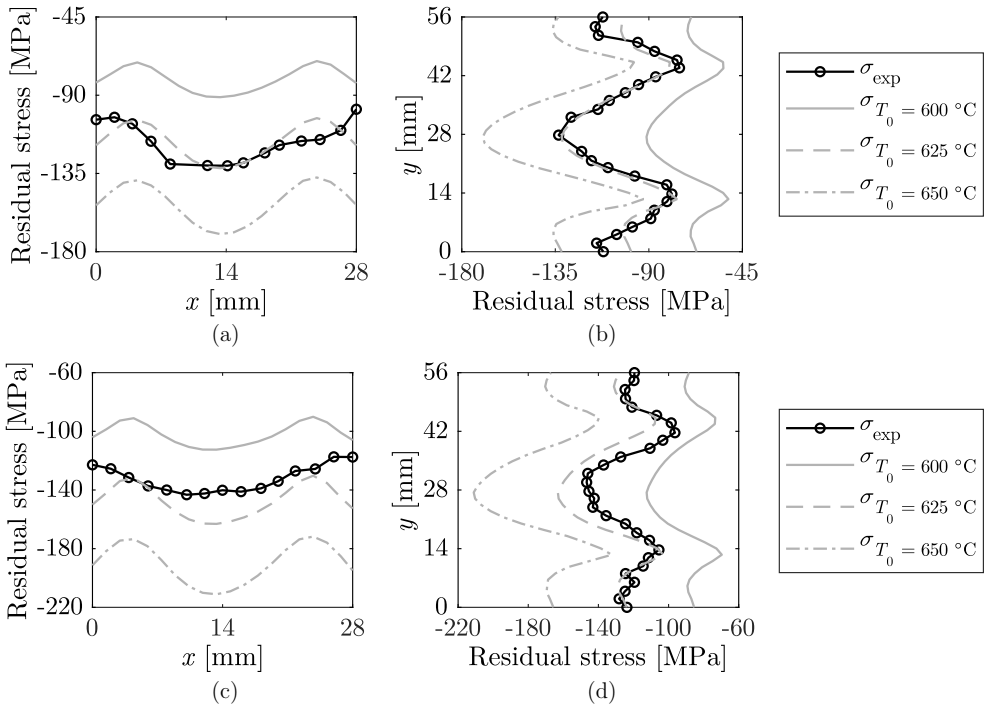

Figure 20: Distribution of absolute maximum principal stresses against experimental data for different glass initial temperatures: 600 °C, 625 °C and 650 °C, along: (a) path *x* with *v* = 100 m/s air flow; (b) path *y* with *v* = 100 m/s air flow; (c) path *x* with *v* = 200 m/s air flow; (d) path *y* with *v* = 200 m/s air flow.

Both, the numerical results and the experimental measurements shared the same trend, as it was able to capture the peaks and troughs caused by the jet pattern in both directions. The difference between the stress amplitudes obtained in the x and y directions may arise from the non-homogeneous heat transfer that occurred on the surface as a result of the defined jet-to-jet distances. The defined jet pitch in x direction made the jet flows to overlap, whereas the larger pitch in the y direction brought about a lower heat extraction between jets, causing the already mentioned dry regions. As a result, the large difference in cooling rate between the jet facing and dry regions led to a large variation in the developed residual stresses between these areas. In both analysed jet velocity cases, the initial temperature of 625 °C seems to be in better agreement with the experimental results. Not surprisingly, this magnitude is considered a common initial temperature value within the glass tempering process [9, 12, 39].

5. Conclusions

A new numerical methodology for calculating the residual stress development in glass plates subjected to non-uniform cooling during the tempering process was presented. The significant conclusions are:

- A generalized FSI numerical procedure to predict non-uniform residual stress distributions in glassware subjected to multiple nozzle or jet arrays was successfully implemented and validated with experimental measurements from the literature. The results showed that local flow phenomena during heat treatment process played a vital role on the residual stress development in glass plates. Consequently, the proposed generalized numerical methodology enabled the calculation of non-uniform residual stress distributions, making it possible to extend its applicability to novel processes such as pulsed jet cooling or interrupt quenching strategies.

- With the aim of seeking a commitment between accuracy and efficiency, different computational cost reduction techniques were assessed. Firstly, the consideration of volumetric radiation tended to homogenize the temperature of the plate as the temperature difference through the thickness was decreased up to 6% for the analysed cases. However, no significant differences were observed in the final residual stress pattern nor in their variation over time. The reason for this may rely on the short period of time that the components remained at high temperature. Additionally, it involved an extremely high computational cost. Hence, volumetric radiation might be neglected throughout the tempering process. However, a more thorough study needs to be carried out when thicker components or lower heat extractions are considered.

- Secondly, the existence of a critical temperature during the tempering process was confirmed. Once the hottest point of the plate was at 400 °C, the subsequent cooling magnitude and distribution was no longer influential and the residual stress development became cooling rate independent within the range from natural to forced convection cooling. In addition, the cooling stage from the critical to room temperature refers to the longest time period of the tempering process, as cooling rate decreases over time. For this reason, the use of a purely thermal model below the critical temperature was proposed in order to reduce the high computational cost that the CFD

calculation entails. To this end, data was transferred to the thermal model where a spatially homogeneous and constant in time HTC was defined.

- Finally, the influence of considering steady and transient HTC on the residual stress pattern was analysed. Deviations in HTC and residual stresses up to 16% and 9%, respectively, were observed in the representative area. As a result, the approach of considering a steady HTC might be a cost-effective solution when crossflow phenomena became negligible. However, differences up to 25% in terms of HTC and 17% in the residual stress magnitudes were observed in the outer area of the plate where crossflow phenomena gained importance. Therefore, it cannot be directly extended to other quenching case studies as the influence of the flow nature should be first evaluated.

- Based on the conclusions of the computational cost reduction analysis, a modified procedure to model low thickness quenching processes seeking a commitment between accuracy and efficiency was proposed. The modified procedure consisted of a transient CFD simulation without volumetric radiation and a purely thermal model once the part was below the critical temperature. The proposed modified methodology provided an efficient tool for understanding the involved multiphysic phenomena and for designing different cooling strategies such as multiple jet cooling, pulsed jets, swirling jets or interrupt quenching techniques. More importantly, the consideration of local flow phenomena might enable the prediction of in-process breakage of the components during cooling. Altogether, these are important issues for future research.

6. Acknowledgments

The authors would like to acknowledge the financial support provided by the Basque Government by means of ICME project (KK- 2021-00021) and Research Groups (IT1505-22 and IT1316).

References

[1] S. R. Ledbetter, A. R. Walker, A. P. Keiller, Structural Use of Glass, Journal of Architectural Engineering 12 (3) (2006) 137–149. doi:10.1061/(ASCE)1076-0431(2006)12:3(137).

[2] M. Haldimann, A. Luible, M. Overend, Structural Use of Glass, IABSE, 2008.

[3] L. H. Adams, E. D. Williamson, The annealing of glass, Journal of the Franklin Institute 190 (5) (1920) 597–631. doi:10.1016/S0016-0032(10)91090-9.

[4] R. Gardon, Thermal Tempering of Glass, in: D. Uhlmann, N. Kreidl (Eds.), Glass Science and Technology, Academic Press, Inc., 1980, pp. 145–216. doi:10.1016/B978-0-12-706705-6.50010-2.

[5] C. Guillemet, Annealing and tempering of glass, Journal of Non-Crystalline Solids 123 (1990) 415–426.

[6] E. H. Lee, T. G. Rogers, T. C. Woo, Residual Stresses in a Glass Plate Cooled Symmetrically from Both Surfaces, Journal of the American Ceramic Society 48 (9) (1965) 480–487. doi:10.1111/j.1151-2916.1965.tb14805.x.

[7] O. S. Narayanaswamy, R. Gardon, Calculation of Residual Stresses in Glass, Journal of the American Ceramic Society 52 (10) (1969) 554–558. doi:10.1111/j.1151-2916.1969.tb09163.x.

[8] O. S. Narayanaswamy, Model of Structural Relaxation in Glass, Journal of the American Ceramic Society 54 (10) (1971) 491–498. doi:10.1111/j.1151-2916.1971.tb12186.x.

[9] O. S. Narayanaswamy, Stress and structural relaxation in tempering glass, Journal of the American Ceramic Society 61 (3-4) (1978) 146–152.

[10] F. P. Incropera, D. P. Dewitt, T. L. Bergman, A. S. Lavine, Fundamentals of heat and mass transfer, sixth edit Edition, no. 1986, John Wiley & Sons, 2007. arXiv:1105-, doi:10.1109/TKDE.2004.30.

[11] H. Carre, L. Daudeville, Numerical Simulation of Soda-Lime Silicate Glass Tempering, Journal de Physique IV 6 (1996) 175–185.

[12] L. Daudeville, H. Carré, Thermal tempering simulation of glass plates: Inner and edge residual stresses, Journal of Thermal Stresses 21 (6) (1998) 667–689. doi:10.1080/01495739808956168.

[13] F. Bernard, R. Gy, L. Daudeville, Finite element computation of residual stresses near holes in tempered glass plates, in: XIX Int. Congr. Glass, Vol. 43C, Edinburgh, 2002, pp. 290–295. doi:10.4028/www.scientific.net/MSF.404-407.43.

[14] F. Bernard, L. Daudeville, Point fixings in annealed and tempered glass structures: Modeling and optimization of bolted connections, Engineering Structures 31 (4) (2009) 946–955. doi:10.1016/j.engstruct.2008.12.004.

[15] J. H. Nielsen, J. F. Olesen, P. N. Poulsen, H. Stang, Simulation of residual stresses at holes in tempered glass: A parametric study, Materials and Structures/Materiaux et Constructions 43 (7) (2010) 947–961. doi:10.1617/s11527-009-9558-z.

[16] N. Pourmoghaddam, J. H. Nielsen, J. Schneider, Numerical simulation of residual stresses at holes near edges and corners in tempered glass: A parametric study, in: J. Schneider, B. Weller (Eds.), Engineered Transparency, Wiley, 2016.

[17] N. Pourmoghaddam, J. Schneider, Finite-element analysis of the residual stresses in tempered glass plates with holes or cut-outs, Glass Structures & Engineering (February) (2018). doi:10.1007/s40940-018-0055-z.

[18] N. Pourmoghaddam, J. Schneider, Determination of the engine power for quenching of glass by forced convection : simplified model and experimental validation of residual stress levels, Glass Structures & Engineering (2018). doi:10.1007/s40940-018-0078-5.

[19] A. Mikkonen, A. Aronen, M. Rantala, R. Karvinen, Effects of non-uniform heat transfer in a tempering process on glass quality, in: Glass Performance Days GDP 2017, 2017.

[20] F. Monnoyer, D. Lochegnies, Heat transfer and flow characteristics of the cooling system of an industrial glass tempering unit, Applied Thermal Engineering 28 (17-18) (2008) 2167–2177. doi:10.1016/j.applthermaleng.2007.12.014.

[21] J. H. Nielsen, J. F. Olesen, H. Stang, Characterization of the Residual Stress State in Commercially Fully Toughened Glass, Journal of Materials in Civil Engineering 22 (2) (2010) 179–185. doi:10.1061/(asce)0899-1561(2010)22:2(179).

[22] J. Anton, A. Errapart, M. Paemurru, D. Lochegnies, S. Hödemann, H. Aben, On the inhomogeneity of residual stresses in tempered glass panels, Estonian Journal of Engineering 18 (1) (2012) 3. doi:10.3176/eng.2012.1.01.

[23] Y. Chen, D. Lochegnies, R. Defontaine, J. Anton, H. Aben, R. Langlais, Measuring the 2D residual surface stress mapping in tempered glass under the cooling jets: The influence of process parameters on the stress homogeneity and isotropy, Strain 49 (1) (2013) 60–67. doi:10.1111/str.12013.

[24] R. Karvinen, A. Aronen, Influence of Cooling Jets on Stress Pattern and Anisotropy in Tempered Glass, in: Glass Performance Days GPD 2019, 2019.

[25] A. Aronen, Modelling of Deformations and Stresses in Glass Tempering, Ph.D. thesis, Tampere Univerisity of Technology (2012).

[26] A. Aronen, R. Karvinen, Effect of glass temperature before cooling and cooling rate on residual stresses in tempering, Glass Structures and Engineering 3 (1) (2018) 3–15. doi:10.1007/s40940-017-0053-6.

[27] N. Zuckerman, N. Lior, Jet impingement heat transfer: Physics, correlations, and numerical modeling, Advances in Heat Transfer 39 (C) (2006) 565–631. doi:10.1016/S0065-2717(06)39006-5.

[28] M. Wannassi, F. Monnoyer, Fluid flow and convective heat transfer of combined swirling and straight impinging jet arrays, Applied Thermal Engineering 78 (2015) 62–73. doi:10.1016/j.applthermaleng.2014.12.043.

[29] N. Sozbir, S. C. Yao, Spray mist cooling heat transfer in glass tempering process, Heat and Mass Transfer 53 (5) (2017) 1699–1711. doi:10.1007/s00231-016-1930-2.

[30] K. H. Lee, R. Viskanta, Quenching of flat glass by impinging air jets, Numerical Heat Transfer; Part A: Applications 33 (1) (1998) 5–22.

doi:10.1080/10407789808913925.

[31] M. F. Modest, Radiative Heat Transfer, 2nd Edition, Academic Press, Inc., 2003.

[32] R. Siegel, Transient Thermal Effects of Radiant Energy In Semitransparent Materials, Journal of Heat Transfer 120 (1998) 4–23. doi:10.2514/1.16842.

[33] N. Siedow, D. Lochegnies, F. Béchet, P. Moreau, H. Wakatsuki, N. Inoue, Axisymmetric modeling of the thermal cooling, including radiation, of a circular glass disk, International Journal of Heat and Mass Transfer 89 (2015) 414–424. doi:10.1016/j.ijheatmasstransfer.2015.04.091.

[34] K. Agboka, F. Béchet, N. Siedow, D. Lochegnies, Influence of radiative heat transfer model on the computation of residual stresses in glass tempering process, International Journal of Applied Glass Science 9 (2) (2018) 235–251. doi:10.1111/ijag.12335.

[35] J. H. Nielsen, Tempered Glass: -Bolted Connections and Related Problems, Ph.D. thesis, Technical University of Denmark (2009). doi:10.1016/j.carres.2009.08.031.

[36] R. Gardon, Calculation of Temperature Distributions in Glass Plates Undergoing Heat-Treatment, Journal of the American Ceramic Society 41 (6) (1958) 200–209. doi:10.1111/j.1151-2916.1958.tb13541.x.

[37] N. Siedow, T. Grosan, D. Lochegnies, E. Romero, Application of a new method for radiative heat transfer to flat glass tempering, Journal of the American Ceramic Society 88 (8) (2005) 2181–2187. doi:10.1111/j.1551-2916.2005.00402.x.

[38] K. H. Lee, R. Viskanta, Two dimensional combined conduction and radiation heat transfer: comparison of the discrete ordinates method and the diffusion approximation methods, Numerical Heat Transfer (39) (2001) 205–225.

[39] J. H. Nielsen, J. F. Olesen, P. N. Poulsen, H. Stang, Finite element implementation of a glass tempering model in three dimensions, Computers and Structures 88 (17-18) (2010) 963–972. doi:10.1016/j.compstruc.2010.05.004.

[40] O. Narayanaswamy, Annealing of glass, in: D. Uhlmann, N. Kreidl (Eds.), Glass: Science and Technology - Viscosity and Relaxation, Academic Press, Inc., 1986, pp. 275–318.

[41] A. Q. Tool, Relation Between Inelastic Deformability and Thermal Expansion of Glass in Its Annealing Range, Journal of the American Ceramic Society 29 (9) (1946) 240–253. doi:10.1111/j.1151-2916.1946.tb11592.x.

[42] R. A. McMaster, Flat Glass Tempering - How It Works, Glass Industry (1989) 10–15.

[43] ANSYS Inc., ANSYS FLUENT Theory Guide Release 18.2 (2017). arXiv:ArXivID, doi:10.1016/0140-3664(87)90311-2.

[44] K. Petera, M. Dostál, Heat transfer measurements and CFD simulations of an impinging jet, EPJ Web of Conferences 114 (2016). doi:10.1051/epjconf/201611402091.

[45] V. Nicolau, F. P. Maluf, Determination of radiative properties of commercial glass, The 18th Conference on Passive and Low Energy Architecture (November) (2001) 5.

[46] Y. Cengel, M. Boles, Appendix 1: Property tables and charts, in: M. Hill (Ed.), Heat and Mass Transfer, 4th Edition, Mexico, 2011, p. 884.